Available online at www.sciencedirect.com

ScienceDirect

Advances in Space Research 57 (2016) 2385–2395

ADVANCES IN SPACE RESEARCH (a COSPAR publication)

www.elsevier.com/locate/asr

Raman–Mössbauer–XRD studies of selected samples from "Los Azulejos" outcrop: A possible analogue for assessing the alteration processes on Mars

E.A. Lalla [a,b,*], A. Sanz-Arranz [b], G. Lopez-Reyes [b], A. Sansano [b], J. Medina [b], D. Schmanke [c], G. Klingelhoefer [c], J.A. Rodríguez-Losada [d], J. Martínez-Frías [e], F. Rull [b]

[a] *Extreme Light Infrastructure – Nuclear Physics (ELI-NP), Horia Hulubei National Institute of Physics and Nuclear Engineering (IFIN HH), 30 Reactorului Street, P.O. Box MG-6, 077125 Magurele, jud. Ilfov, Romania*

[b] *Unidad Asociada UVa-CSIC al Centro de Astrobiología, Edificio INDITI, Parque Tecnológico de Boecillo, 47151 Boecillo, Valladolid, Spain*

[c] *Institut für Anorganische Chemie und Analytische Chemie, Johannes Gutenberg, Universität Mainz, 55099 Mainz, Germany*

[d] *Departamento de Biología Animal, Edafología y Geología, Universidad de la Laguna, 38200 San Cristóbal de La Laguna, Santa Cruz de Tenerife, Spain*

[e] *Dinámica Terrestre y Observación de la Tierra, Instituto de Geociencias, IGEO (CSIC-UCM), Facultad de Ciencias Geológicas, Ciudad Universitaria, 28040 Madrid, Spain*

Received 27 April 2015; received in revised form 7 March 2016; accepted 8 March 2016
Available online 16 March 2016

Abstract

The outcrop of "Los Azulejos" is visible at the interior of the Cañadas Caldera in Tenerife Island (Spain). It exhibits a great variety of alteration processes that could be considered as terrestrial analogue for several geological processes on Mars. This outcrop is particularly interesting due to the content of clays, zeolite, iron oxides, and sulfates corresponding to a hydrothermal alteration catalogued as "Azulejos" type alteration. A detailed analysis by portable and laboratory Raman systems as well as other different techniques such as X-ray diffraction (XRD) and Mössbauer spectroscopy has been carried out (using twin-instruments from Martian lander missions: Mössbauer spectrometer MIMOS-II from the NASA-MER mission of 2001 and the XRD diffractometer from the NASA-MSL Curiosity mission of 2012). The mineral identification presents the following mineral species: magnetite, goethite, hematite, anatase, rutile, quartz, gregoryite, sulfate (thenardite and hexahydrite), diopside, feldspar, analcime, kaolinite and muscovite. Moreover, the in-situ Raman and Micro-Raman measurements have been performed in order to compare the capabilities of the portable system specially focused for the next ESA Exo-Mars mission. The mineral detection confirms the sub-aerial alteration on the surface and the hydrothermal processes by the volcanic fluid circulations in the fresh part. Therefore, the secondary more abundant mineralization acts as the color agent of the rocks. Thus, the zeolite–illite group is the responsible for the bluish coloration, as well as the feldspars and carbonates for the whitish and the iron oxide for the redish parts. The XRD system was capable to detect a minor proportion of pyroxene, which is not visible by Raman and Mössbauer spectroscopy due to the "Azulejos" alteration of the parent material on the outcrop. On the other hand, Mössbauer spectroscopy was capable of detecting different types of iron-oxides ($Fe^{3+/2+}$-oxide phases). These analyses emphasize the strength of the different techniques and the working synergy of the three different techniques together for planetary space missions.

Keywords: Raman; Mars; Alteration processes; Mineralogy; Volcanic analogues

* Corresponding author at: Extreme Light Infrastructure – Nuclear Physics (ELI-NP), Horia Hulubei National Institute of Physics and Nuclear Engineering (IFIN HH), 30 Reactorului Street, P.O. Box MG-6, 077125 Magurele, jud. Ilfov, Romania. Tel.: +40 214042300.
E-mail address: Emmanuel.lalla@eli-np.ro (E.A. Lalla).

http://dx.doi.org/10.1016/j.asr.2016.03.014
0273-1177/

1. Introduction

Several volcanic places have been used as possible terrestrial analogues taking into account the volcanic activities and the huge variety of geological processes discovered on Mars heretofore (Chevrier and Mathé, 2007) such as Hawaiian Island, Marion Island, among others (Graham et al., 2015; Prinsloo et al., 2011). Considering the previous research, one of the most important alteration processes of volcanic materials on Martian surface are related to the hydrothermal processes (Merle et al., 2010). All the information yielded from the different NASA missions such as the Mars Exploration Rover (MER, (Rayl, 2014)) and the Mars Science Laboratory-Curiosity (MSL, (Kuhn, 2015a)) have improved the understanding of the geological diversity of the planet. However, the possibility of establishing new terrestrial environments as analogue test sites for future space missions such as ESA-ExoMars mission (Bost et al., 2015; Courrèges-Lacoste et al., 2007; Rull-Pérez and Martinez-Frias, 2006) and the future NASA mission in 2020 (Grossman, 2013) is needed. In this regard, new terrestrial volcanic analogue environments can provide new data which could be used for the interpretation of the geological history of Mars and the data collected by the different future space missions (Bishop et al., 2004; Lalla, 2014; Prinsloo et al., 2011). Special attention has to be paid to the mineralogy because it is the best indicator of the physical–chemical geo-processes and the paragenetic assemblages. Thus, the mineral diversity of new terrestrial analogues could allow the scientific community to increase the knowledge about the geological processes throughout the history of Mars (Mouginis-Mark and Robinson, 1992). Examining the Martian mineralogy, it has been observed that it is as rich as the Earth mineralogy showing secondary mineralization such as oxides, phyllosilicates, sulfates, carbonates, zeolites and clays (Chevrier and Mathé, 2007; Lalla et al., 2010; Minitti and Hamilton, 2010; Ruff, 2004). Secondary and accessory minerals have a paragenetic origin from hydrothermal reactions with the sub-surface fluids, water alteration, and sub-aerial processes. Nevertheless, there is a controversy about the detailed processes occurred on Mars, especially with the chemically weathered basalt (Mahaney et al., 2012). The use of natural samples from basaltic terrestrial analogues have been selected to perform future analysis on Mars relevant samples (with which the technology can be tested and improved).

It has been demonstrated that Tenerife Island is an area of reference for carrying out research and technological studies with planetary and astrogeological implications (Lalla et al., 2015). Several places of the island have been selected considering the fluid–rock interactions caused by the weathering processes, the submarine and sub-aerial alteration, hydrothermalism and the geomorphological features (Lalla et al., 2015a,b)

The main motivation of this paper is to study and register a complete spectroscopic analysis (mainly by Raman spectroscopy) of the selected outcrop corresponding to "Los Azulejos", which exhibits visible alterations from the original rocks (called "Azulejos" alteration), and whose results could be used as potential model substances for the original altered material on Mars. On the other hand, the data collected using twin-instrument from present and future different space missions in terrestrial analogues may contribute for the next generation objectives in space exploration. Finally, this study is also focused to improve the strength of the Raman spectroscopy for space exploration and to complement the results with the capabilities of the XRD and Mössbauer techniques.

2. Geological setting

The Cañadas Caldera, at the central part of Tenerife Island, as may indicated by (Marti and Gudmundsson, 2000) was formed by several collapse episodes of the Cañadas central volcanic edifice during several highly explosive eruptions of phonolitic magmas (see Fig. 1). From the geochemical point of view, the Cañadas edifice has been and is also affected by active hydrothermal and fumaloric activities as well as CO_2 diffuse emission (Villasante-Marcos et al., 2014), this has acted after the Caldera formation. The combination of the mechanical and geochemical processes produced a heterogeneous volcanic system, where really interesting specific outcrops could become a terrestrial analogues for instrument testing and contribute to the science development of new space missions. In this regard, one of the most interesting macro-structural formation is the called the outcrop of "Los Azulejos" (Fig. 1), that forms a part of the Caldera wall. One of the most impressive features at this outcrop is the variety of the different processes involved (i.e. hydrothermal processes, argilization and parent mineralogical alteration) (Galindo et al., 2005; Villasante-Marcos et al., 2014). Galindo et al., 2005, have described these geological features indicating that the faults within "Los Azulejos" structure affect the igneous materials of the Cañadas edifice by the inclined and sub-vertical sheets intrusions formation. In addition, it has been reported a variable displacement of the fault is reported in (Galindo et al., 2005). They also point out that the kinetic indicators such as the offset of stratigraphic layers, shear-cleavage structures in mylonitic foliation, among others, in combination with the CO_2 active diffuse degassing activities and the hydrothermal activities cause a huge variety of mineralogical species. The colored outcrop of "Los Azulejos" presents bluish, greenish, whitish, and yellowish colors (Fig. 1). The bluish to greenish degradation corresponds to a combination of analcime and clay minerals such as smectite and illite. On the other hand, yellowish and blank coloration can be observed on the fumarolic structure and the argilization of the parent minerals. These colorations present really interesting formations like mushrooms textures and veins circulation with sulfates and iron oxides mineral species (Bustillo, 1989; Galindo et al., 2005). The colors in the alteration correspond to a process termed "Los Azulejos" type alteration and it is also present on

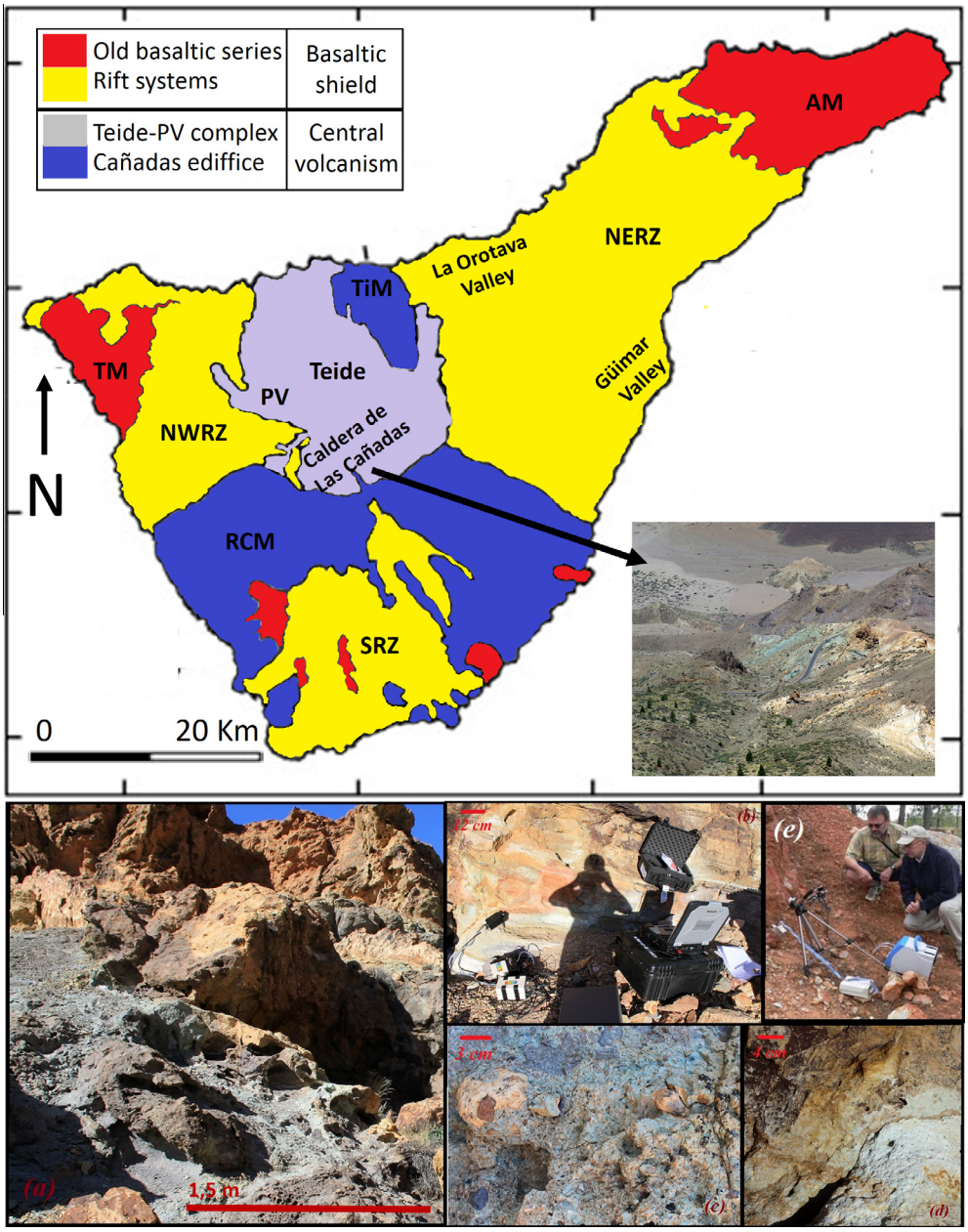

Fig. 1. Simplified geological map of Tenerife illustrating the outcrops of the products from the basaltic shield, the Central Volcanism and geographical situation of the outcrop of "Los Azulejos" (TM: Teno massif; NWRZ: North-west Rift zone; SRZ: South Rift zone; NERZ: North-east Rift zone; TiM: Tigaiga massif; AM: Anaga massif; PV: Pico Viejo; RCM: Roque del Conde massif). (a) Picture of the studied outcrop, (b) portable instrumentation working under field conditions, (c) bluish and greenish coloration, (d) yellowish and whitish coloration, (e) Raman and Mössbauer spectrometers working in synergy under field conditions using a mechanical positioner (credits: ESA). (For interpretation of the references to color in this figure legend, the reader is referred to the web version of this article.)

other Canary Island graben formations such as Gran Canaria Island, Spain (Donoghue et al., 2008).

3. Analytical techniques

3.1. In-situ portable instrumentation

The Raman analyses were performed with an i-Raman device from B&W TEK Inc. designed to work at field conditions (Unidad Asociada UVa-CSIC al Centro de Astrobiología, Valladolid, Spain). The optical system was adapted and positioned in front of the samples using a mechanical positioner, this allows a surface mapping at near mineral grain scale (Fig. 1). A baffle was used to minimize the solar light background. The excitation used was a laser with 532 nm wavelength, 15 mW power on the sample, a spot diameter of 85 μm and the best spectral resolution of 5 cm^{-1}. Some of the zones present a strong effect of the fluorescence, with inconclusive results and these samples have been carefully selected to carry out a Micro-Raman measurement at the Unidad Asociada UVa-CSIC al Centro de Astrobiología.

The Mössbauer spectra were collected with a copy of the Miniaturized Mössbauer spectrometer MIMOS II spectrometer from the past NASA-MER-mission (AK Klingelhoefer, Mars Mössbauer Group, Mainz, Germany). The system has a Co^{57}/Rh source with an intensity of about 50 mCi. The measurements have been performed at room temperature and without sample preparation in a backscattering geometry.

The XRD system for the measurement was the Terra XRD diffractometer instrument (based on the MSL-CheMin concept, available at the Unidad Asociada UVa-CSIC with a detector of 1024×256 pixels, 2D peltier cooled CCD camera for XRD with a source of cobalt X-ray tube, working at 30 kV and 300 μA. For the XRD analysis, a preparation was necessary: powdering a minimum part of the samples (from 2 to 4 mg) and sieving with a granulometry lower than 150 μm. The XRD measurement and analysis were obtained using a 0.25° 2θ° FWHM resolution, a 2θ° spectral range of 5–55° and 200 accumulations with an exposition time of 15 s. The mineral identification software used was the Xpowder12 (Martin-Ramos, 2004).

3.2. Laboratory instrumentation

The micro-Raman mineralogical characterization of the samples was performed with a micro-Raman system from the Unidad Asociada UVa-CSIC. The system is composed by a microscope Nikon Eclipse E600 coupled to a spectrometer KOSI Holospec f/1.8i, with best spectral resolution of 5 cm^{-1}, illuminated by a laser REO LSRP-3501 He–Ne (632.8 nm wavelength). The detector was a CCD Andor DV420A-OE-130. The maximum laser power used on the sample was 14 mW with a minimum spot diameter of 15 μm. The Raman mapping of the bulk surface of the sample was done by the micro-Raman Prior Proscan II motorized stage in automatic mode in order to detect the different compositional mineralization. However, the optimum recording conditions were obtained by varying the laser power, microscope objective, and the confocal spot size (XY instrument) as required for the different samples. The spectra have been directly acquired on the sample material without any sample preparation.

The conventional X-ray diffraction analyses were carried out at University of Valladolid, Spain with a XRD diffractometer Philips PW1710 equipped with an automatic divergent slit graphite monochromator and Cu-anode. Experimental conditions: $Cu_{K\alpha}$ radiation, $\lambda = 0.154$ nm, a nickel filter, an aluminum sample-holder, 40 kV generator voltage, generator current 30 mA with a relation intensity of 0.5 (α_1/α_2), and angle range (2θ°) from 5° to 70°. The steps size applied is 0.02° and the identification has been done using Match! Program system, the crystallography Open Database (COD), the ICDD System (International Centre for Diffraction Data) in PDF-2 (Power Diffraction Files), and the JCPDS (Joint Committee on Powder diffraction Standards).

4. Results

4.1. Sample recollection and description

The samples from the different places of the in-situ analysis have been collected according to the coloration and characterized by the laboratory instrumentation at the Unidad Asociada UVa-CSIC and at Mars Mössbauer Group, Mainz, Germany. Moreover, the selected samples present different grain size, color, morphological characteristics, and stratigraphic position which are visually distinctive to the human and under microscope magnification. A total of 14 samples have been collected using a hammer and the blade of knife carefully stored in plastic bags to avoid/minimize possible contamination. Table 1 presents the pictures, cataloguing, the general Raman analysis and XRD of each sample collection.

4.2. Raman analysis

The in-situ Raman analysis can be observed in Fig. 2 and the laboratory measurement is presented in Fig. 3. Moreover, the complete mineral species are depicted on Table 1. The identification of the mineral species has been done considering the following references: Fe-oxides (Jubb and Allen, 2010; Rull et al., 2007), Ti-oxides (Lukačević et al., 2012; Sekiya et al., 2001), Si-oxides (Karwowski et al., 2013; Zotov et al., 1999), carbonates (Buzgar and Apopei, 2009; Koura et al., 1996), sulfates (Buzgar et al., 2009; Chio et al., 2005), silicates (Freeman et al., 2008), zeolites (Chen et al., 2007; Frost et al., 2014) and clays (Frost et al., 2001; Haley et al., 1982; Martens et al., 2002) (see Table 2). Also, the RUFF database and the Unidad Asociada spectra collection have been used for the identification (Downs et al., 2015).

The iron oxides detected on the outcrop correspond to hematite, goethite, and magnetite. The detection has been done considering the principal active Raman vibrations of each mineral. The vibrations exhibited by the magnetite were at 670, 550, and 300 cm^{-1} approximately which can be assigned to the following modes A_{1g}, T_{2g}, and E_g vibrational modes (Jubb and Allen, 2010; Rull et al., 2007). In the case of the hematite, the Raman principal vibrations modes are produced at 225 (A_{1g}), 245 (E_g), 291 (E_g), 410 (E_g), 500 (A_{1g}), and 611 (E_g) cm^{-1} with the magnon at 1321 ($2E_u$) cm^{-1}. The goethite presents a combination of several vibrations at 244 (E_g), 299 (E_g), 385 (E_g), 480 (A_{1g}), 550 (A_{1g}), and 681 (E_g) cm^{-1} (Hanesch, 2009). The Ti-oxides detected on the different samples correspond to anatase and rutile. According to the factor group analysis, the anatase has six Raman active modes ($A_{1g} + 2B_{1g} + 3E_g$) allowed to appear at 145 (E_g), 200 (E_g), 393 (B_{1g}), 512 (A_{1g}), 520 (B_{1g}), and 640 cm^{-1} (E_g) (Rull et al., 2007). However, the rutile phase presents only four Raman-active modes at 235 (B_{1g}), 448 (E_g), 609 (A_{1g}), and 810 cm^{-1} (B_{2g}) (Rull et al., 2007; Sekiya et al., 2001).

Table 1
Resume of samples selected, cataloguing and mineralogical detection by Raman spectroscopy and XRD. The majority of the samples have been analyzed at the Unidad Asociada Laboratory and the most interesting samples have been analyzed by Mössbauer Spectroscopy by the MIMOS-II twin system.

Sample	Cataloguing	Raman results	XRD results
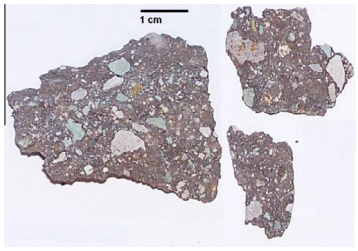	AZLJ-01	Goethite Hematite Anatase Quartz Sulfate Orthoclase Anorthoclase Analcime Kaolinite	Magnetite Anatase Fe-Oxides Quartz Silica Feldspar Zeolite Kaolinite
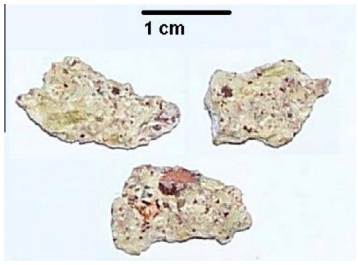	AZLJ-02	Hematite Magnetite Anatase Quartz Gregoryite Anorthoclase Oligoclase Albite Analacime Muscovite	 Quartz Silica Oligoclase Albite Sanidine Zeolite
	AZLJ-03	Magnetite Hematite Goethite Anatase Quartz Thernardite Hexydrite Albite Feldspar Analcime	 Magnetite Diopside Analcime Feldspar Quartz Ti-Oxide Zeolite Muscovite
	AZLJ-04	Magnetite Goethite Hematite Anatase Rutile Quartz Gregoryite Thernardite Feldspar Kaolinite Muscovite	 Anatase Ti-oxides Pyroxene Feldspar Sanidine Albite Zeolite

The carbonate detected can correspond to hydrotalcite, being a Al–Mg rich hydrous carbonate, which has several modes at 237, 288, 484, 700, 1026, 1062, and 1370 cm^{-1} according to the references (Frost et al., 2005). The most intense vibration at 1062 cm^{-1} corresponds to the C—O stretching in the CO_3 bonded to Al^{3+}-bond-OH groups followed with a shoulder at 1050 cm^{-1} (caused by C—O stretching in CO_3 bonded to Mg^{2+}-bond OH group). The other intense peak group from 720 to 650 cm^{-1} are assigned to the CO_3 in-plane bending mode. However, other authors (Buzgar and Apopei, 2009; Buzgar et al., 2009) present similar vibrations as the detected which can correspond to an anhydrous K-carbonate. The doublet bands at 1064 and 1048 cm^{-1} can be assigned to the $\nu_1(A_1)$ stretching modes-CO_3^{2-} and the 1306 and 701 cm^{-1} bands are assigned to the $\nu_3(E')$ – symmetric CO stretching mode and the $\nu_4(E')$ – COH bending mode (Buzgar and Apopei, 2009; Buzgar et al., 2009).

In the case of the sulfates, several mineral phases have been detected corresponding to the thenardite and hexahydrite that can be easily detected by the SO_4 vibrational modes and also by the H_2O vibrational bands. The peaks

Table 2
List of detected minerals characterized by Raman spectroscopy and its general chemical formula.

Type	Mineral	Chemical formula	Raman principal bands (cm^{-1})
Fe-Oxide and Oxy-hydroxide	Magnetite	Fe_3O_4	550, 670
	Hematite	Fe_2O_3	295, 607, 1315
	Goethite	α-FeO(OH)	248, 296, 386, 550, 682
Ti-Oxide	Anatase	TiO_2	393, 512, 635
	Rutile	TiO_2	235, 448, 609, 810
Carbonates	Gregoryite	$(Na_2, K_2, Ca)CO_3$	700, 1062, 1370
Sulfate	Thenardite	$NaSO_4{\cdot}10H_2O$	624, 635, 650,992, 1100, 1131, 1154
	Hexahydrite	$MgSO_4{\cdot}6H_2O$	478, 617, 996
Silicates	Quartz	SiO_2	463
	Orthoclase	$KAlSi_3O_8$	280, 454, 473, 512
	Anorthoclase	$(Na, K)AlSi_3O_8$	456, 474, 511
	Sanidine	$(K, Na)(Si, Al)_4O_8$	456, 470, 511
	Oligoclase	$(Na, Ca)(Si, Al)_4O_8$	480, 508
	Anorthite	$CaAl_2Si_2O_8$	471, 487, 509
	Albite	$NaAlSi_3O_8$	459, 507
Zeolite	Analcime	$Na(AlSi_2O_6){\cdot}H_2O$	384, 480, 1100
Clays	Kaolinite	$Al2Si_2O_5(OH)_4$	258, 333, 393, 461, 510, 640
	Muscovite	$KAl_2(AlSi_3O_{10})(OH)_2$	290, 406, 700, 1100

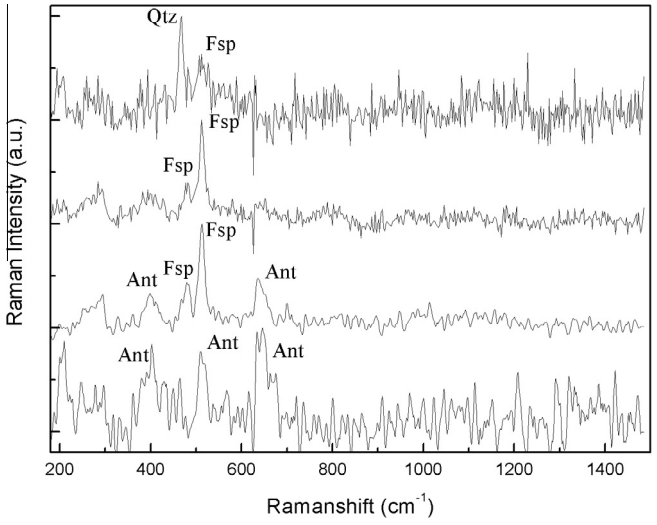

Fig. 2. In-situ Raman spectra from the selected samples obtained from the outcrop of "Los Azulejos". Mineral identification: Quartz (Qtz), anatase (Ant) and feldspar (Fsp).

within water stretching and bending modes of the hexahydrite are shown at around 3450/3250 and 1650 cm^{-1} (Wang et al., 2006). However the major interest is more focused on the SO_4 vibrations at 983 (ν_1), 466 (ν_2), 1146 (ν_3) 610 (ν_1) and at 364 cm^{-1} (no detected) according to the other authors (Wang et al., 2006). On the other hand, the thenardite, which is an anhydrous sulfate, presents the principal band at 991 (ν_1), a doublet at 463/450 (ν_2), a triplet band at 1110/1129/1153/ (ν_3) and other triplet at 620/631/545 cm^{-1} (ν_1) (Wang et al., 2006). In our case, the thenardite has been better detected because it presents a better crystalline structure than the hexahydrite. This has been fairly compared to the RUFF database (Downs et al., 2015).

The identification process of the feldspars and plagioclases has been done based on a band fitting method to overcome the overlapping of Raman signals with other mineral species. The classification method developed by other authors was applied (Freeman et al., 2008), where the strongest vibrational bands are produced by the structure of SiO_4 of tecto-silicate group and it is characterized by triplet or doublet bands located on the 450–515 cm^{-1} region with the strongest peak is at 505–515 cm^{-1}. Also, other vibrational regions have been considered for the correct mineral identification such as: (1) the rotational–translational modes (200–400 cm^{-1}) (2) the deformation modes of the tetrahedral (600–800 cm^{-1}) and (3) the region of the vibrational stretching mode of the tetrahedral structure 900–1200 cm^{-1} (Freeman et al., 2008). However, this identification depends upon the sample under analysis due to some of the spectra matches with the references in some case, but in others were necessary the use of the RUFF database (Downs et al., 2015). The different types of feldspars are indicative of different cation contents in the solid solution expected in basaltic material formation.

The analcime presents the main following vibrations: (1) the water librations E_g at 390 cm^{-1} (2) the O—(Al, Si)—O bending E_g at 480 cm^{-1} (3) the (Al, Si)—O stretching F_{2g} at 1100 cm^{-1} (Frost et al., 2014). Concerning the clays, two types were detected: (1) kaolinite and (2) muscovite. The first clay (kaolinite) vibrations match with the results from other measurements carried out by other authors. The main Raman bands are at 290, 406, and 700 cm^{-1} that are assigned to: the lattice vibrations, the Al–O–Al vibrations (symmetrical stretching vibrations are the strongest vibrations) and the Si–O–Si vibrations at the teatrahedral

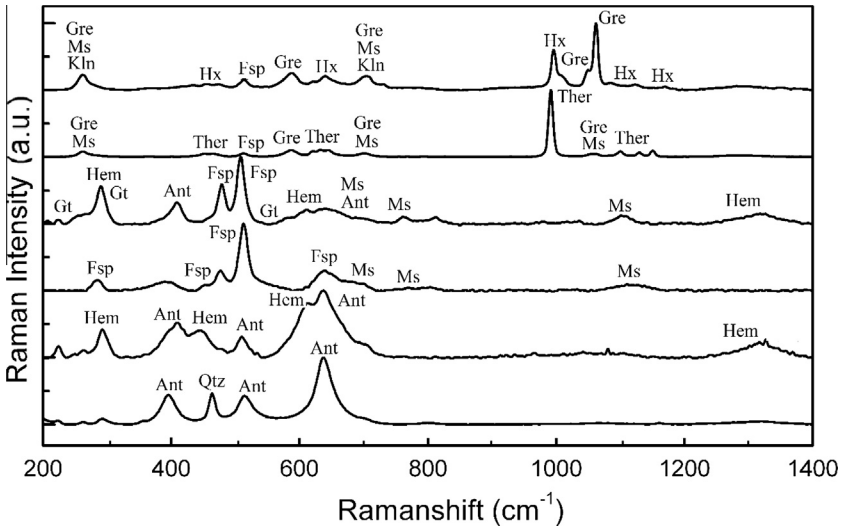

Fig. 3. Micro-Raman spectra from the selected samples obtained from the outcrop of "Los Azulejos". Mineral identification: Quartz (Qtz), anatase (Ant), feldspar (Fsp), hematite (Hem), muscovite (Ms), thenardite (Ther), goethite (Gt), gregoryite (Gre), kaolinite (Kln) and hexahydrite (Hx).

Table 3
Mössbauer fitting parameters of the spectra in the Fig. 4. IS: isomer shift; Γ: experimental line width and QS: quadrupole splitting parameter.

Sample	IS (mm/s)	QS (mm/s)	Γ (mm/s)
Fitting using Lorentzian lineshapes with cosine smearing correction Yellowish Coloration			
Hematite	0.24	16.20	0.14
Goethite	0.54	17.06	0.33
$Fe^{3+/2+}$ oxide phase	0.14	0.51	0.23
Fitting using Lorentzian line shapes with cosine smearing correction Bluish-greenish Coloration			
$Fe^{3+/2+}$ oxide phase	0.13	0.56	0.22

site (Haley et al., 1982). For last, the kaolinite present several active Raman bands at 258, 333, 393, 461, 510, and 640 cm^{-1} (Frost et al., 2001).

4.3. XRD diffraction analysis

The XRD analyses of several samples are shown in Figs. 4 and 5. The identifications have been obtained by pattern matching and taking into consideration the main bands of the diffractograms using the methods aforementioned. Also, the analysis of both diffraction systems converges that they present several crystalline structures with some minor amorphous phases. Furthermore, the results have been compared with other commercial standard patterns. However, the XRD could detect other mineral structure like the diopside, which can be related due to a very low proportion or a low crystal size for the Raman techniques. For the different samples, the majority of the mineral phases have been obtained being similar to the Raman measurements

4.4. Mössbauer spectroscopy

Mössbauer spectroscopy analysis has been performed measuring the different colored areas of the samples as done with XRD. The hyperfine parameter, derived from the data, is depicted in Table 3 and Fig. 6. The different sub-spectral areas obtained by a band fitting from the different samples show Fe oxide-content. Moreover, the $Fe^{3+/2+}$ oxide phases present on the different samples have a similar isomer shift (IS), quadrupole splitting (QS) and spectral line width (Fleischer et al., 2012). The observed presence of hematite, magnetite, goethite, and oxide phase with different degrees of crystallinity have been also confirmed by Raman analyses and XRD.

5. Discussion of the results

The Raman analysis shows the primary mineralization and it is also confirmed by XRD measurement such as the feldspar. On the other hand, the Fe-oxides has been confirmed by Mössbauer spectroscopy like the hematite, magnetite, and goethite. The Raman identifications have been carefully done by the peak assignment of the principal bands, by several methods developed by other authors, by comparison with internal and external database. The in-situ analysis shows, in several case, strong activities of fluorescence that maybe caused by external contamination due to biological activities or saturation caused by large exposition. However, other difficulties have to be considered from the technological point of view such as that some constituents from basaltic rocks have their own fluores-

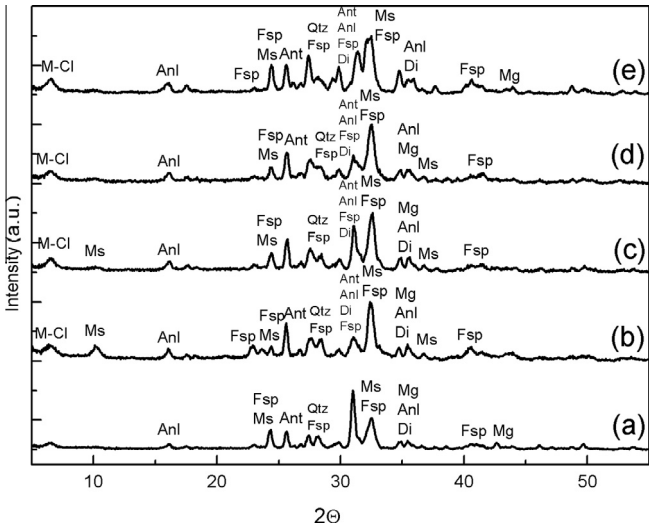

Fig. 4. Terra-InXitu CheMin XRD difractogram from the outcrop of "Los Azulejos" of some selected samples. (a) Powdered bluish sample (AZLJ-01), (b and c) powdered yellowish-whitish sample (AZLJ-02) and (d and e) powdered greenish sample (AZLJ-03). Mineral identification: Muscovite (Ms), diopside (Di), analcime (Anl), quartz (Qtz), feldspar (Fsp), anatase (Ant), magnetite (Mg) and clays (M-Cl).

cence (Bathgate et al., 2015). In this regard, other authors proposed to stablish specific methodologies for the identification and the diagnosis of the peaks in order to mitigate this effect (Bathgate et al., 2015; Wang et al., 1994). But, in the case of remote planetary laboratories, they cannot be applied because of the limitation in the capabilities. Thus, a greater understanding and greater quantity of in-situ spectra from terrestrial analogues are needed for the success of the future space missions. On the other hand, the XRD supplementary technique have shown to be more powerful than the Raman techniques in the mineral identification with a 88% success rate than 77% rate. Nevertheless, if the fluorescence effect is eliminated on Raman techniques, it can be possible to achieve 90% success rate (Bathgate et al., 2015). The main motivation of using a 532 nm portable Raman system is due to the Raman Laser System (RLS) onboard on the ESA-ExoMars that will be working with the same wavelength. In this regard, previous studies using the RLS simulator working at 532 nm shows that the system was capable of detecting the secondary materials directly related with the different alteration processes. However, the laser power has to be chosen carefully as a trade-off between general instrument performance and the risk of damaging thermolabile mineral species (Lalla et al., 2013).

In the geological considerations, the analogue outcrop presented shows strong mineral similarities with the long term and earliest volcanology of Mars. In this point of view, the Martian surface present extensive partial melting mineral with unaltered basalt and low evidence of evolved siliceous rocks. The main justification is the absence of plate tectonics on the Martian surface that prevent the cycling of material as found on Earth (Christensen et al., 2003; Kuhn, 2015b; Sigurdsson et al., 1999). However, the earliest Martian volcanic activity, in the recent discoveries, has been more influenced by explosive eruptions. Thus, the large quantities of volatiles or the presence of ground water have been responsible for the hydrothermal and the fumarolic activities with its mineral alteration (Chevrier and Mathé, 2007; Mangold et al., 2007). In this regard, the fumarolic activity and their diffuse emission processes presented on the outcrop of "Los Azulejos" with the formation of hydrothermal sulfate minerals could be used as a parent model for the alteration processes aforementioned. The sulfates on the outcrop of "Los Azulejos"

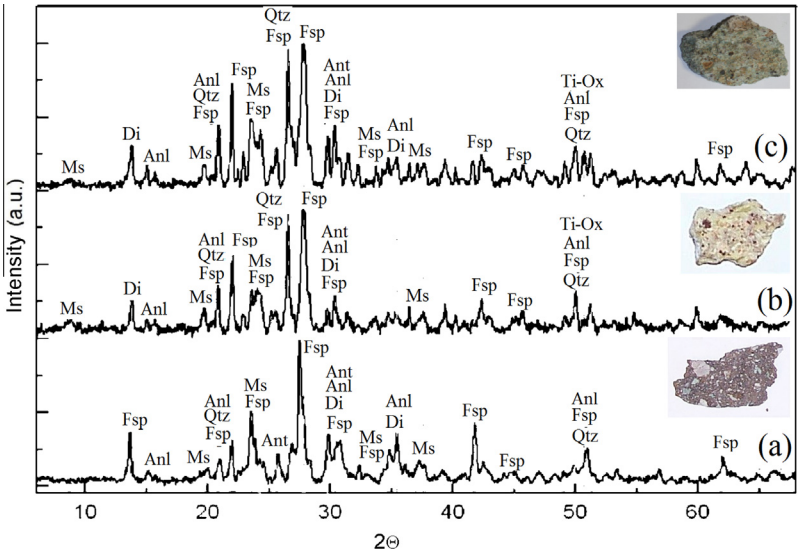

Fig. 5. Laboratory XRD difractogram from the outcrop of "Los Azulejos" of some selected samples. (a) Powdered bluish sample (AZLJ-01), (b) powdered yellowish-whitish sample (AZLJ-02) and (c) powdered greenish sample (AZLJ-3). Mineral identification: Muscovite (Ms), diopside (Di), analcime (Anl), quartz (Qtz), feldspar (Fsp), anatase (Ant) and Ti-oxide (Ti-Ox). (For interpretation of the references to color in this figure legend, the reader is referred to the web version of this article.)

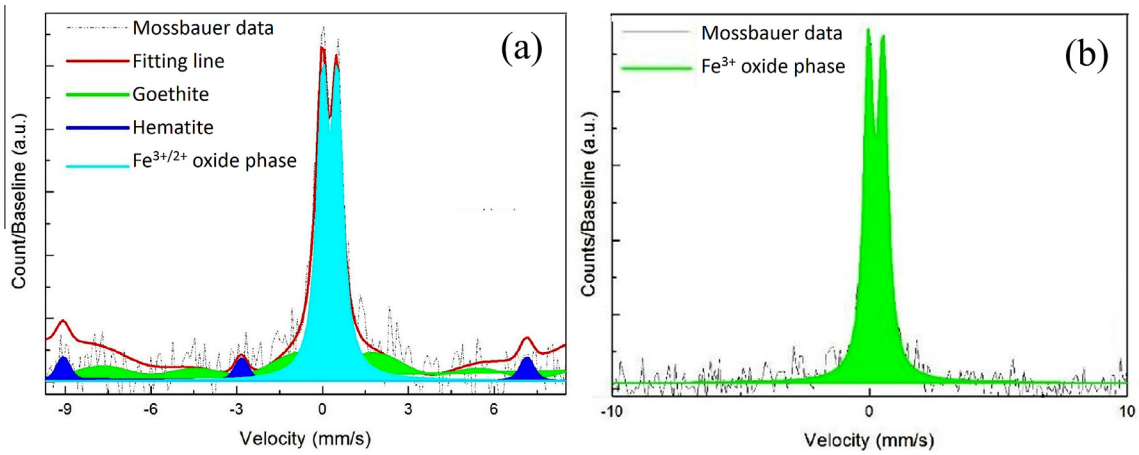

Fig. 6. Representative Mössbauer spectra from the outcrop of "Los Azulejos" observed on the fitting process of the experimental data presenting the weathering phases such as hematite, goethite and Fe^{3+} phases. (a) Yellowish coloration sample and (b) bluish-greenish coloration sample. (For interpretation of the references to color in this figure legend, the reader is referred to the web version of this article.)

Table 4
Comparison of the capabilities of the three systems employed on this investigation.

Technique	Structural identification	Elemental composition	Geological context	Penetration capability
Raman spectroscopy	Yes	Potentially	Yes	No
XRD	Yes	No	Potentially	No
Mössbauer Spectroscopy	Only with Fe-content materials	No	Yes	Yes

are products of the interaction of magmatic fluids, volcanic gases (H_2S and SO_2), and the surrounding rocks. They can be of interest for future studies and to increase our knowledge of the processes occurred over the Martian geological time. Taking into account the recent space missions like NASA-Curiosity mission and NASA-MER-mission, where twin instruments have been used in this investigation, present similar mineral phases (Anderson et al., 2015; Klingelhöfer et al., 2003). Moreover, the minerals detected on Mars are in accordance with our investigations on the outcrop of "Los Azulejos", and this could be of importance for future testing of Raman spectrometers of Martian automatic laboratories. Also, our Raman results encourage to the continue development of Raman systems within space science and for the Mars exploration. A comparison of the different techniques is available on Table 4 showing the capabilities of the Raman spectroscopy applied to the geological context. Its combination with the other techniques shows that they are capable to obtain a full detail of the mineralogy and the geological process occurred on the selected target.

6. Conclusions

Different measurements have been performed by in-situ and laboratory Raman spectroscopic techniques, X-ray diffractometers and Mössbauer spectrometer for the very first time on the outcrop of "Los Azulejos", through a complete analysis of the mineralogy. Regarding to this, its possible relation to Mars based on its possible alteration processes has been also studied. Crystalline primary phases such as pyroxene, feldspar, oxides as well as secondary minerals like carbonate, Fe-oxides/oxy-hydroxides, sulfates, zeolites, and clays have been confirmed by Raman spectroscopy and XRD analyses. Moreover, the Mössbauer spectroscopy also detected Fe-oxides and other amorphous $Fe^{3+/2+}$ oxide phases as a result of hydrothermal alteration. The phases of mineral species described along the paper are similar to those reported on other volcanic terrestrial analogue materials and Martian observations. The possibility to distinguish between different alteration processes by Raman spectroscopy will help us to deduce the rock-process formation by the combined processes occurred on the outcrop of "Los Azulejos" and its possible extension to Mars. Thus, the enlargement of knowledge on terrestrial analogues provide an aid and a relevant knowledge support for the planetary research field, especially when astrogeological implications are addressed. The results reveal that Raman technique, XRD, and Mössbauer spectroscopy are powerful and robust systems. The three techniques in combination will be suitable for a complete identification of alteration processes inferred on Mars. In this regard, the measurements support the continued endeavors of the system developments for the Mars exploration on the future space mission such as the Raman Laser Spectrometer (RLS) included in the ESA Exo-Mars Mission. However, a continued improvement of the Raman technique is needed for the success of the future space missions

Acknowledgements

The work was supported by the MICINN with the Project AYA-2008-04529 for the development of the Raman-LIBS combined spectrometer for the ESA-ExoMars Mission. Emmanuel Lalla thanks MICINN for the FPI grant (BES-2009-024992). The authors also want to thank Prof. Dr. F. García Talavera for the logistic organization and collaboration during the fieldtrip to the Museo del Hombre y la Naturaleza, (Tenerife Spain) and to Parques Nacionales – Gobierno de Canarias, (Tenerife, Spain).

References

Anderson, R., Bridges, J.C., Williams, A., Edgar, L., Ollila, A., Williams, J., Nachon, M., Mangold, N., Fisk, M., Schieber, J., Gupta, S., Dromart, G., Wiens, R., Le Mouélic, S., Forni, O., Lanza, N., Mezzacappa, A., Sautter, V., Blaney, D., Clark, B., Clegg, S., Gasnault, O., Lasue, J., Léveillé, R., Lewin, E., Lewis, K.W., Maurice, S., Newsom, H., Schwenzer, S.P., Vaniman, D., 2015. ChemCam results from the Shaler outcrop in Gale crater, Mars. Icarus 249, 2–21. http://dx.doi.org/10.1016/j.icarus.2014.07.025.

Bathgate, E.J., Maynard-Casely, H.E., Caprarelli, G., Xiao, L., Stuart, B., Smith, K.T., Pogson, R., 2015. Raman, FTIR and XRD study of Icelandic tephra minerals: implications for Mars. J. Raman Spectrosc. 46, 846–855. http://dx.doi.org/10.1002/jrs.4694.

Bishop, J.L., Murad, E., Lane, M.D., Mancinelli, R.L., 2004. Multiple techniques for mineral identification on Mars: a study of hydrothermal rocks as potential analogues for astrobiology sites on Mars. Icarus 169, 311–323. http://dx.doi.org/10.1016/j.icarus.2003.12.025.

Bost, N., Ramboz, C., LeBreton, N., Foucher, F., Lopez-Reyes, G., De Angelis, S., Josset, M., Venegas, G., Sanz-Arranz, A., Rull, F., Medina, J., Josset, J.-L., Souchon, A., Ammannito, E., De Sanctis, M. C., Di Iorio, T., Carli, C., Vago, J.L., Westall, F., 2015. Testing the ability of the ExoMars 2018 payload to document geological context and potential habitability on Mars. Planet. Space Sci. 108, 87–97. http://dx.doi.org/10.1016/j.pss.2015.01.006.

Bustillo, M.A., 1989. Alteración Hidrotermal en los Azulejos, in: Araña, V., Coello, J. (Eds.), Los Volcanes Y La Caldera Del Parque Nacional Del Teide. pp. 311–314.

Buzgar, N., Apopei, A.I., 2009. The Raman Study on Certain Carbonates. Analele Stiint. ale Univ. "Al. I. Cuza", Iasi, pp. 97–112, vol. 55.

Buzgar, N., Buzatu, A., Sanislav, I.V., 2009. The Raman Study on Certain Sulfates. Analele Stiint. ale Univ. "Al. I. Cuza", pp. 5–23, vol. 55.

Chen, Y., Zhou, Y., Zhang, L., Wu, M., Yan, S., 2007. Discovery of CH_4-rich high-pressure fluid inclusions hosted in analcime from Dongying depression. China J. Pet. Sci. Eng. 56, 311–314. http://dx.doi.org/10.1016/j.petrol.2006.10.005.

Chevrier, V., Mathé, P.E., 2007. Mineralogy and evolution of the surface of Mars: a review. Planet. Space Sci. 55, 289–314. http://dx.doi.org/10.1016/j.pss.2006.05.039.

Chio, C.H., Sharma, S.K., Muenow, D.W., 2005. Micro-Raman studies of hydrous ferrous sulfates and jarosites. Spectrochim. Acta, Part A: Mol. Biomol. Spectrosc. 61, 2428–2433. http://dx.doi.org/10.1016/j.saa.2005.02.021.

Christensen, P.R., Bandfield, J.L., Bell III, J.F., Gorelick, N., Hamilton, V.E., Ivanov, A., Jakosky, B.M., Kieffer, H.H., Lane, M.D., Malin, M.C., McConnochie, T., McEwen, A.S., McSween, H.Y., Mehall, G. L., Moersch, J.E., Nealson, K.H., Rice, J.W., Richardson, M.I., Ruff, S.W., Smith, M.D., Titus, T.N., Wyatt, M.B., 2003. Morphology and composition of the surface of Mars: Mars odyssey THEMIS results. Science 300, 2056–2061. http://dx.doi.org/10.1126/science.1080885.

Courrèges-Lacoste, G.B., Ahlers, B., Rull Perez, F., 2007. Combined Raman spectrometer/laser-induced breakdown spectrometer for the next ESA mission to Mars. Spectrochim. Acta, Part A: Mol. Biomol. Spectrosc. 68, 1023–1028. http://dx.doi.org/10.1016/j.saa.2007.03.026.

Donoghue, E., Troll, V.R., Harris, C., O'Halloran, A., Walter, T.R., Pérez Torrado, F.J., 2008. Low-temperature hydrothermal alteration of intra-caldera tuffs, Miocene Tejeda caldera, Gran Canaria, Canary Islands. J. Volcanol. Geotherm. Res. 176, 551–564. http://dx.doi.org/10.1016/j.jvolgeores.2008.05.002.

Downs, B., Robinson, S., Yang, H., Mooney, P., 2015. RRUFF Project. Dep. Geosci. Univ, Arizona.

Fleischer, I., Klingelhöfer, G., Morris, R.V., Schröder, C., Rodionov, D., de Souza, P.A., 2012. In-situ Mössbauer spectroscopy with MIMOS II. Hyperfine Interact. 207, 97–105.

Freeman, J.J., Wang, A., Kuebler, K.E., Jolliff, B.L., Haskin, L.A., 2008. Characterization of natural feldspars by Raman spectroscopy for future planetary exploration. Can. Mineral. 46, 1477–1500. http://dx.doi.org/10.3749/canmin.46.6.1477.

Frost, R.L., Fredericks, P.M., Kloprogge, J.T., Hope, G.A., 2001. Raman spectroscopy of kaolinites using different excitation wavelengths. J. Raman Spectrosc. 32, 657–663. http://dx.doi.org/10.1002/jrs.722.

Frost, R.L., Adebajo, M.O., Erickson, K.L., 2005. Raman spectroscopy of synthetic and natural iowaite. Spectrochim. Acta, Part A: Mol. Biomol. Spectrosc. 61, 613–620. http://dx.doi.org/10.1016/j.saa.2004.05.015.

Frost, R.L., López, A., Theiss, F.L., Romano, A.W., Scholz, R., 2014. A vibrational spectroscopic study of the silicate mineral analcime – $Na_2(Al_4SiO_4O_{12})\cdot 2H_2O$ – A natural zeolite. Spectrochim Acta, Part A: Mol. Biomol. Spectrosc. 133, 521–525. http://dx.doi.org/10.1016/j.saa.2014.06.034.

Galindo, I., Soriano, C., Martí, J., Pérez, N., 2005. Graben structure in the Las Cañadas edifice (Tenerife, Canary Islands): Implications for active degassing and insights on the caldera formation. J. Volcanol. Geotherm. Res. 144, 73–87. http://dx.doi.org/10.1016/j.jvolgeores.2004.11.017.

Graham, L., Graff, T.G., Aileen Yingst, R., ten Kate, I.L., Russell, P., 2015. 2012 Moon Mars analog mission activities on Mauna Kea, Hawaii. Adv. Space Res. 55, 2405–2413. http://dx.doi.org/10.1016/j.asr.2015.01.024.

Grossman, L., 2013. NASA urged to seek live Martians with 2020 rover. New Sci. 219, 9. http://dx.doi.org/10.1016/S0262-4079(13)61775-3.

Haley, L.V., Wylie, I.W., Koningstein, J.A., 1982. An investigation of the lattice and interlayer water vibrational spectral regions of muscovite and vermiculite using Raman microscopy. A Raman microscopic study of layer silicates. J. Raman Spectrosc. 13, 203–205. http://dx.doi.org/10.1002/jrs.1250130217.

Hanesch, M., 2009. Raman spectroscopy of iron oxides and (oxy) hydroxides at low laser power and possible applications in environmental magnetic studies. Geophys. J. Int. 177, 941–948. http://dx.doi.org/10.1111/j.1365-246X.2009.04122.x.

Jubb, A.M., Allen, H.C., 2010. Vibrational spectroscopic characterization of hematite, maghemite, and magnetite thin films produced by vapor deposition. ACS Appl. Mater. Interfaces 2, 2804–2812. http://dx.doi.org/10.1021/am1004943.

Karwowski, Ł., Helios, K., Kryza, R., Muszyński, A., Drożdżewski, P., 2013. Raman spectra of selected mineral phases of the Morasko iron meteorite. J. Raman Spectrosc. 44, 1181–1186. http://dx.doi.org/10.1002/jrs.4340.

Klingelhöfer, G., Morris, R.V., Bernhardt, B., Rodionov, D., de Souza, P. A., Squyres, S.W., Foh, J., Kankeleit, E., Bonnes, U., Gellert, R., Schröder, C., Linkin, S., Evlanov, E., Zubkov, B., Prilutski, O., 2003. Athena MIMOS II Mössbauer spectrometer investigation. J. Geophys. Res. Planets 108. http://dx.doi.org/10.1029/2003JE002138.

Koura, N., Kohara, S., Takeuchi, K., Takahashi, S., Curtiss, L.A., Grimsditch, M., Saboungi, M.-L., 1996. Alkali carbonates: Raman spectroscopy, ab initio calculations, and structure. J. Mol. Struct. 382, 163–169. http://dx.doi.org/10.1016/0022-2860(96)09314-3.

Kuhn, N., 2015. Experiments in Reduced Gravity. Elsevier, Experiments in Reduced Gravity, doi: 10.1016/B978-0-12-799965-4.00002-9.

Kuhn, N., 2015b. Chapter 2 – Overview of Mars, in: Kuhn, N.B.T.-E. in R.G. (Ed.), Experiments in Reduced Gravity. Elsevier, Oxford, pp. 17–26. doi: http://dx.doi.org/10.1016/B978-0-12-799965-4.00002-9.

Lalla, E., 2014. Tenerife como análogo de Marte: Caracterización multianalítica (Raman, DRX, ATR-FTIR, SEM y MossBaeur) de muestras de interés planetario y astrobiológico. Dep. Física la Mater. Condens. Cristalogr. y Minerealogía – Univ. Valladolid, University of Valladolid.

Lalla, E., Caramazana Sansano, A., Sanz-Arranz, A., Alonso Alonso, P., Medina García, J., Martinez-frías, J., Rull-Perez, F., 2010. Espectroscopía Raman de Basaltos Correspondientes al Volcán de Las Arenas. Tenerife. MACLA – Soc. Española Mineral. 13, 129–130.

Lalla, E., Lopez-Reyes, G., Rull, F., Medina, J., Martinez-Frias, J., Sansano, A., Navarro, R., 2013. Raman analysis of basaltic samples from Tenerife Island (Cañadas, Azulejos, and Historical eruptions) with the ExoMars RLS instrument, in: 44th Lunar and Planetary Science Conference. Houston, Texas, p. 2403.

Lalla, E.A., López-Reyes, G., Sansano, A., Sanz-Arranz, A., Martinez-Frías, J., Medina, J., Rull-Pérez, F., 2015. Raman-IR vibrational and XRD characterization of ancient and modern mineralogy from volcanic eruption in Tenerife Island: Implication for Mars. Geosci. Front. http://dx.doi.org/10.1016/j.gsf.2015.07.009.

Lalla, E.A., López-Reyes, G., Sansano, A., Sanz-Arranz, A., Schmanke, D., Klingelhöfer, G., Medina-García, J., Martínez-Frías, J., Rull-Pérez, F., 2015. Estudio espectroscópico y DRX de afloramientos terrestres volcánicos en la isla de Tenerife como posibles análogos de la geología marciana. Estud. Geológicos 71, 1–19. http://dx.doi.org/10.3989/egeol.41927.354.

Lukačević, I., Gupta, S.K., Jha, P.K., Kirin, D., 2012. Lattice dynamics and Raman spectrum of rutile TiO_2: The role of soft phonon modes in pressure induced phase transition. Mater. Chem. Phys. 137, 282–289. http://dx.doi.org/10.1016/j.matchemphys.2012.09.022.

Mahaney, W.C., Fairén, A.G., Dohm, J.M., Krinsley, D.H., 2012. Weathering rinds on clasts: examples from Earth and Mars as short and long term recorders of paleoenvironment. Planet. Space Sci. 73, 243–253. http://dx.doi.org/10.1016/j.pss.2012.08.025.

Mangold, N., Poulet, F., Mustard, J.F., Bibring, J.P., Gondet, B., Langevin, Y., Ansan, V., Masson, P., Fassett, C., Head, J.W., Hoffmann, H., Neukum, G., 2007. Mineralogy of the Nili Fossae region with OMEGA/Mars express data: 2. Aqueous alteration of the crust. J. Geophys. Res. E Planets 112.

Martens, W.N., Ding, Z., Frost, R.L., Kristof, J., Kloprogge, J.T., 2002. Raman spectroscopy of hydrazine-intercalated kaolinite at 77, 298, 323, 343 and 358 K. J. Raman Spectrosc. 33, 31–36. http://dx.doi.org/10.1002/jrs.812.

Marti, J., Gudmundsson, A., 2000. The Las Cañadas Caldera (Tenerife, Canary Islands): an overlapping collapse caldera generated by magma-chamber migration. J. Volcanol. Geotherm. Res. 103, 161–173. http://dx.doi.org/10.1016/S0377-0273(00)00221-3.

Martin-Ramos, J.D., 2004. XPowder: A Software Package for Powder X-Ray Diffraction Analysis Powder Methods.

Merle, O., Barde-Cabusson, S., van Wyk de Vries, B., 2010. Hydrothermal calderas. Bull. Volcanol. 72, 131–147. http://dx.doi.org/10.1007/s00445-009-0314-6.

Minitti, M.E., Hamilton, V.E., 2010. A search for basaltic-to-intermediate glasses on Mars: assessing Martian crustal mineralogy. Icarus 210, 135–149. http://dx.doi.org/10.1016/j.icarus.2010.06.028.

Mouginis-Mark, P., Robinson, M., 1992. Evolution of the Olympus mons caldera. Mars Bull. Volcanol. 54, 347–360. http://dx.doi.org/10.1007/BF00312318.

Prinsloo, L.C., Colomban, P., Brink, J.D., Meiklejohn, I., 2011. A Raman spectroscopic study of the igneous rocks on Marion Island: a possible terrestrial analogue for the geology on Mars. J. Raman Spectrosc. 42, 626–632. http://dx.doi.org/10.1002/jrs.2756.

Rayl, A.J.S., 2014. Mars Exploration Rovers Update: Mission Nears 10-Year Milestone, Oppy Roves On, We Look Back on 2013 [WWW Document]. Planet. Soc. URL http://www.planetary.org/explore/space-topics/space-missions/mer-updates/2013/12-mer-update-mission-nears-10-year-milestone.html.

Ruff, S.W., 2004. Spectral evidence for zeolite in the dust on Mars. Icarus 168, 131–143. http://dx.doi.org/10.1016/j.icarus.2003.11.003.

Rull, F., Martinez-Frias, J., Rodríguez-Losada, J.A., 2007. Micro-Raman spectroscopic study of El Gasco pumice, western Spain. J. Raman Spectrosc. 38, 239–244. http://dx.doi.org/10.1002/jrs.1628.

Rull-Pérez, F., Martinez-Frias, J., 2006. Raman spectroscopy goes to Mars. Spectrosc. Eur. 18, 18–21.

Sekiya, T., Ohta, S., Kamei, S., Hanakawa, M., Kurita, S., 2001. Raman spectroscopy and phase transition of anatase TiO_2 under high pressure. J. Phys. Chem. Solids 62, 717–721. http://dx.doi.org/10.1016/S0022-3697(00)00229-8.

Sigurdsson, H., Bruce, H., Rymer, H., John, S., McNutt, S., 1999. Encyclopedia of Volcanoes. Academic Press.

Villasante-Marcos, V., Finizola, A., Abella, R., Barde-Cabusson, S., Blanco, M.J., Brenes, B., Cabrera, V., Casas, B., De Agustín, P., Di Gangi, F., Domínguez, I., García, O., Gomis, A., Guzmán, J., Iribarren, I., Levieux, G., López, C., Luengo-Oroz, N., Martín, I., Moreno, M., Meletlidis, S., Morin, J., Moure, D., Pereda, J., Ricci, T., Romero, E., Schütze, C., Suski-Ricci, B., Torres, P., Trigo, P., 2014. Hydrothermal system of Central Tenerife volcanic complex, Canary Islands (Spain), inferred from self-potential measurements. J. Volcanol. Geotherm. Res. 272, 59–77. http://dx.doi.org/10.1016/j.jvolgeores.2013.12.007.

Wang, A., Han, J., Guo, L., Yu, J., Zeng, P., 1994. Database of standard Raman spectra of minerals and related inorganic crystals. Appl. Spectrosc. 48, 959–968.

Wang, A., Freeman, J.J., Jolliff, B.L., Chou, I.-M., 2006. Sulfates on Mars: a systematic Raman spectroscopic study of hydration states of magnesium sulfates. Geochim. Cosmochim. Acta 70, 6118–6135. http://dx.doi.org/10.1016/j.gca.2006.05.022.

Zotov, N., Ebbsjö, I., Timpel, D., Keppler, H., 1999. Calculation of Raman spectra and vibrational properties of silicate glasses: comparison between $Na_2Si_4O_9$ and SiO_2 glasses. Phys. Rev. B. http://dx.doi.org/10.1103/PhysRevB.60.6383.